

Passive Charge Modulation for a Wireless Pressure Sensor

Authors:

Charles Theurer: Department of Mechanical Engineering,
University of Massachusetts, Amherst

Li Zhang: Department of Mechanical Engineering,
University of Massachusetts, Amherst

David Kazmer: Department of Plastics Engineering,
University of Massachusetts, Lowell

Robert Gao: Department of Mechanical Engineering,
University of Massachusetts, Amherst

Robert Jackson: Department of Electrical and Computer Engineering,
University of Massachusetts, Amherst

Abstract:

A wireless pressure sensor is described for use in a high pressure manufacturing process with three major sub-systems: energy conversion by a stack of piezoelectric disks, energy measurement and control by a threshold modulator, and ultrasonic signal transmission by a piezoelectric transmitter. The second system, the threshold modulator, is the focus of this paper. The charge, proportional to pressure, on a capacitive element is measured and controlled through the use of a two transistor modulator. Standard NPN and PNP transistors are used to passively control the flow of charge between a piezoelectric stack and an ultrasonic transmitter. The basis for the design is discussed, from which a simulation is developed and compared to a bench top prototype. The results of this comparison indicate appropriateness of the assumptions used to produce an analytical model of the design and the limiting conditions under which the modulator will effectively measure charge. Finally the prototype device is optimized with respect to sensitivity, gain, and operating range for use in real time process monitoring and control.

Introduction

Most complex commercial products are manufactured by net shape manufacturing processes [1] in which an amorphous feed stock is deformed into a permanent shape. In these processes, such as injection molding and die casting, the internal state of the process is distributed with respect to time and space. As such, these commercial processes typically proceed in an open loop fashion with respect to the process states, with limited observability and controllability. In development of control systems for these manufacturing processes, the value of information must be weighed against its cost.

In general, the closer the sensor is to the forming mechanisms, the more valuable the information is to process control [2]. However, in many manufacturing processes the cost associated with getting the information increases with its proximity to the process due to heightened requirements related to geometry, temperature, and stress. This is particularly true in injection molding where mold complexity and requirements make it expensive to instrument molds individually. Thus sensing has been traditionally done at fixed locations in the injection machine such as hydraulic pressure behind the screw but not directly within the mold or mold cavity. The cost of instrumentation originates from three sources: (1) the initial cost of the sensor, (2) the cost of installation, and (3) the cost of maintenance. Complex injection molds typically include moving cores, cooling lines, and modular cavity inserts that increase the installation and maintenance costs which, over the life of a sensor, may far exceed its initial cost [3].

As evidenced by their use, wireless sensors have been widely successful in reducing the installation and maintenance cost associated with process control. However

such an approach is precluded in net shape manufacturing processes such as injection molding primarily because of the operating conditions of the process and the structurally required use of electromagnetically opaque materials in these molds. One solution to the wireless sensor transmission problem is the use of ultrasonic telemetry in place of electromagnetic telemetry. Unlike their electromagnetic counterparts, ultrasonic waves travel very effectively through most conventional metals such as steel and aluminum [4]. The cost of maintenance is further reduced for the wireless sensor by making it self-powered. Self-powering is enabled through the extraction of available energy in the process being measured to power the sensor (Figure 1). The development of wireless sensors is intended to increase the number of sensors used for process control by reducing the initial cost per sensor and allowing the installation of sensors without major mold modifications compared to traditional cabled sensors.

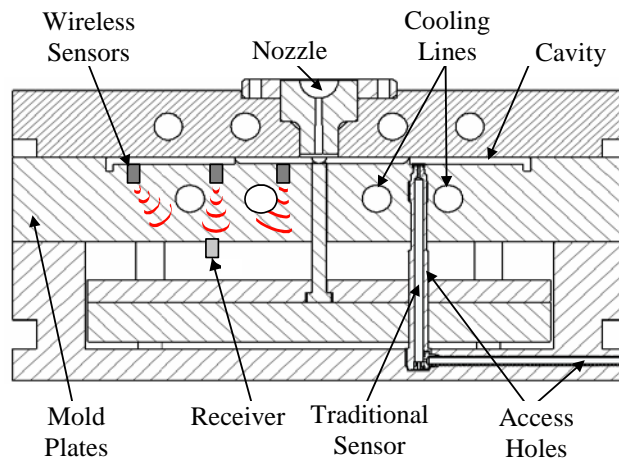


Figure 1. Injection mold instrumented with the wireless sensor system (left) and a traditional wired sensor (right)

As shown in Figure 2, a self-powered wireless sensor was proposed by the authors [5] and consists of two major physical components: (1) a wireless sensing unit and (2) a receiving unit. The wireless sensing unit is installed from the cavity side of the injection

mold and is in contact with the polymer as the cavity fills. The energy converter changes the transient melt pressure differential into electrical energy proportional to the pressure change in the cavity. The threshold modulator controls the flow of energy between the converter and an ultrasonic transmitter. When the energy stored in a capacitive element in the modulator is below its threshold, the modulator electrically resembles an open switch. Once the stored charge reaches the predetermined voltage threshold, corresponding to a predetermined pressure change, the modulator changes state, to resemble a closed switch, and sends that energy in the form of a high current electrical pulse to an ultrasonic transmitter. The energy is there converted to ultrasonic waves that travel through the injection mold to a receiver located on the outside of the injection mold. The pulses from one or multiple wireless sensing units are counted, multiplied by the known pressure threshold and a pressure profile is reconstructed.

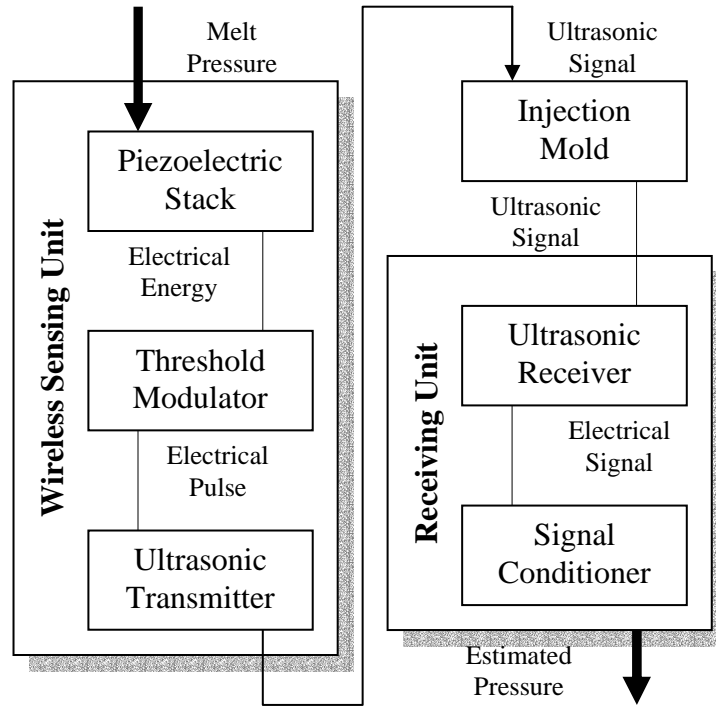


Figure 2. Signal path functional decomposition of the wireless sensor system

The remainder of this paper investigates the design and operation of the threshold modulator and is laid out as follows. First, the threshold modulator design is presented. Second, a simulation of the threshold modulator is developed. Next, the performance of the threshold modulator is discussed with respect to operating parameters. The design is then implemented and compared to simulation. Finally, the threshold modulator bench top device is optimized to maximize operating range through selection of device parameters.

Threshold Modulator Design

A model of the wireless sensing unit is presented in Figure 3. The piezoelectric stack is modeled as a current source. In this representation, charge is proportional to change in pressure and therefore current is expressed as;

$$I_o = SC \frac{dp}{dt} \quad \text{Equation 1.}$$

where I_o is the current from the current source, SC is the stack constant (related to the material and geometric properties of the stack), and dp/dt is the time derivative of pressure. This analysis is appropriate at frequencies below the natural frequency of the device [6] and is valid here because the natural frequency of the device, $\vartheta(10^6 \text{ Hz})$, is much greater than the frequency of the process, $\vartheta(10^2 \text{ Hz})$. Charge is stored in both the stack and in the modulator capacitance; the former is capacitance inherent in the piezoelectric stack [7] while the latter is a design parameter.

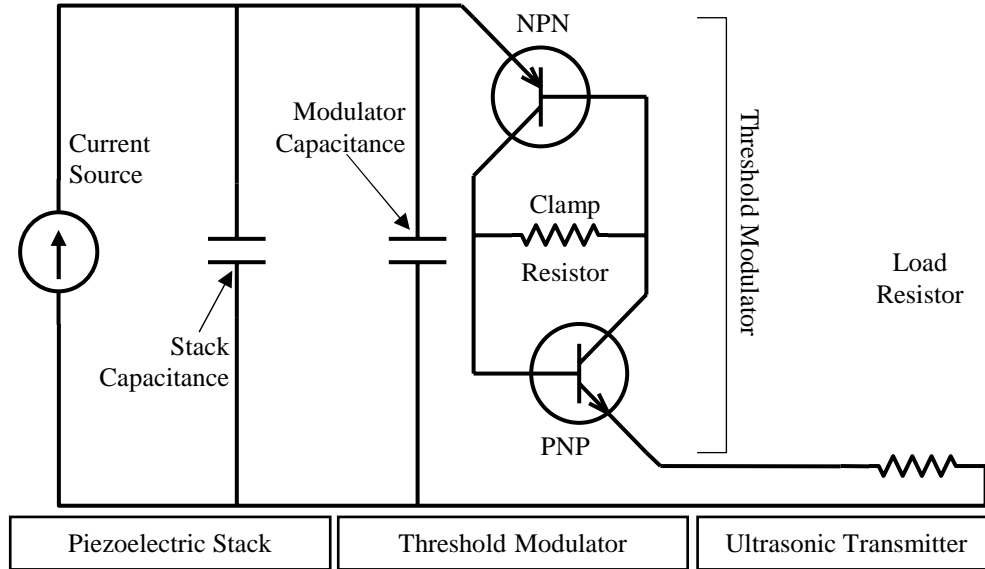


Figure 3. Schematic diagram of the threshold modulator with an electrical simplification of the piezoelectric stack and the ultrasonic transmitter

A change in pressure is converted to a charge by the piezoelectric stack. Once the voltage across the piezoelectric stack reaches a given threshold, the modulator converts that charge to a current pulse transmitted through the ultrasonic transmitter. In a typical design, the threshold voltage is around 1.2 V. This threshold level, combined with the sensitivity of the energy converter, determines the possible sensor resolution. For example, using a 10-ring stack energy converter described previously [8], the sensor resolution would be approximately 43 kPa, which corresponds to an 11 bit sensor for a typical operating pressure of 100Mpa. This performance compares well with traditional strain-based sensors that have a typical accuracy of 0.1%.

The voltage current behavior of an ideal modulator is shown in Figure 4. The ideal threshold modulator transmits zero current in the open (off) state below the threshold voltage, (Figure 4, points a to b). It ideally has no resistance in the closed (on) state when the current is above the shutoff current (Figure 4, point c). In the (on) state,

the charge stored on the stack and modulator capacitor is allowed to flow through the threshold modulator. Once the voltage on the capacitive elements reaches some lower threshold or shutoff voltage, the modulator current goes below the shutoff current and the ideal threshold modulator then reverts to an off state (Figure 4, point d). As long as the pressure on the stack is increasing, the charge will again begin to accumulate and the state of the switch will repeat the loop (Figure 4, points b-c-d).

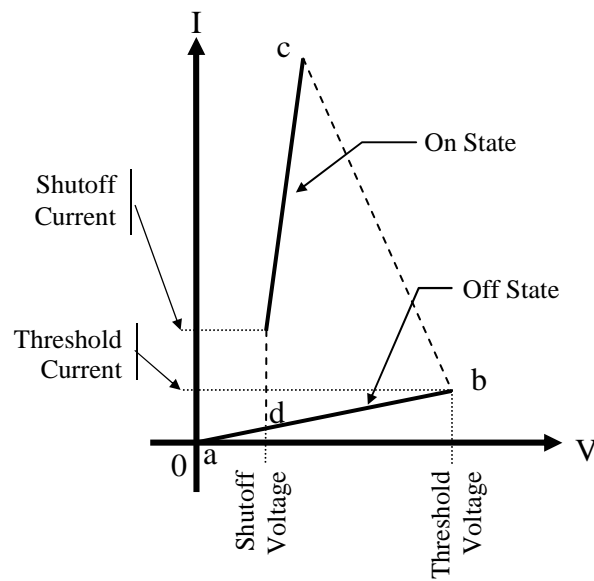


Figure 4. Current voltage curve for an ideal threshold modulator

Discussion of the Threshold Modulator

Circuit Parameters

A modulator was designed based on the dynamics of a relaxation oscillator. A simulation of the circuit in Figure 5 was carried out in order to understand the switching process (Figure 4 points b-c-d). The details of the circuit are as follows: The current source I_s is a constant value of 0.05ma, the equivalent combined capacitor value C_e is

60.5nF, the clamp resistor value R is 2.0K Ω , the load resistor value R_1 is 100 Ω , and the PNP transistor model (Q1) is a Fairchild 2N2907A, while the NPN transistor model (Q2) is a Fairchild 2N2222. I_x is the current through the modulator, V_x is the voltage across the modulator, and V_o is the voltage across the load resistor R_1 .

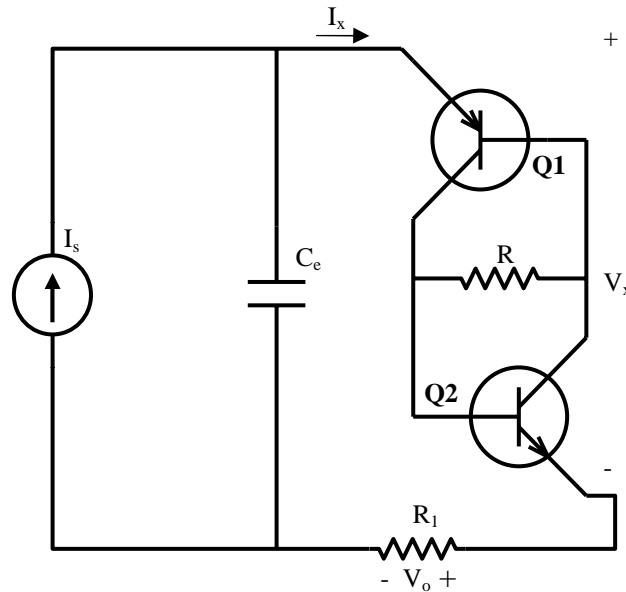


Figure 5. Schematic diagram of the evaluation circuit for the threshold modulator

Modulator Signal Dynamics

The simulated IV characteristic curve for the modulator is plotted in Figure 6 in order to compare the ideal IV characteristic curve in Figure 4 with the simulated results of the circuit in Figure 5. The low resistance off state from point a to b, the negative slope of the IV curve (negative resistance) from point b to c as well as the turn off at point d are the salient characteristics associated with the ideal IV curve of Figure 4 and are present in the simulation results presented in Figure 6.

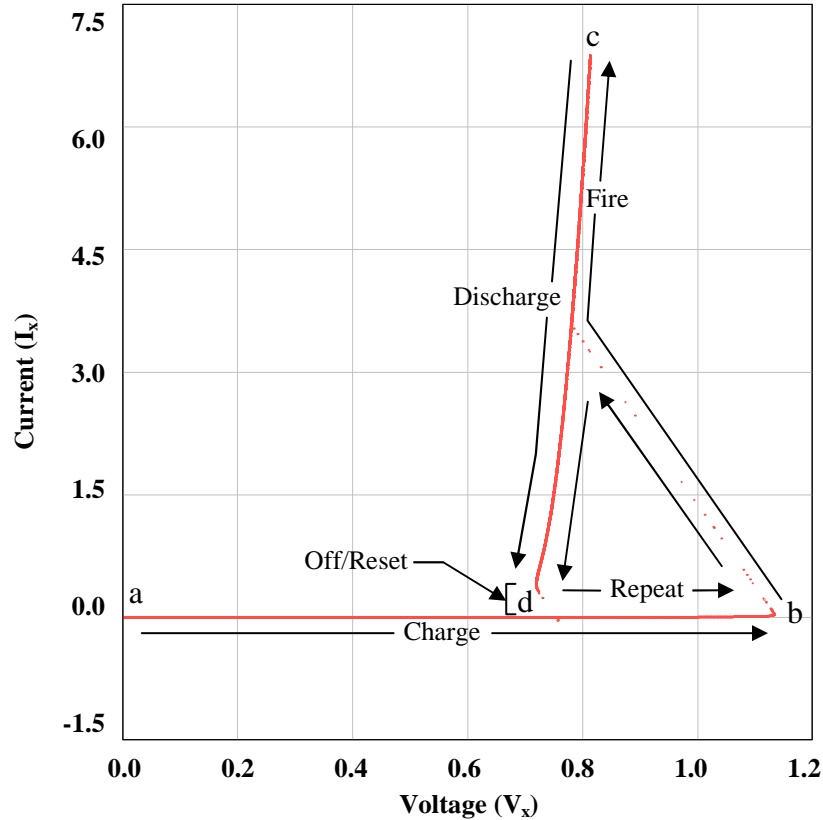


Figure 6. The IV characteristic curve for the simulated threshold modulator

The resulting dynamics of the circuit can be broken down into the four distinct phases illustrated in Figure 7. Phase one includes the time that the modulator is in its off state and the capacitive elements are *charging*. Phase two begins at t_0 and includes a very short time where the threshold modulator changes from its relative off state to its relative on state. Phase three begins at time t_1 and includes the time that the modulator is in its relative on state while the capacitive elements *discharge* through the modulator and load transmitter until time t_2 . After time t_2 the transistors turn *off* and *reset* while the capacitive elements begin to charge again. A detailed explanation of the operation of the threshold modulator with respect to time follows Figure 7.

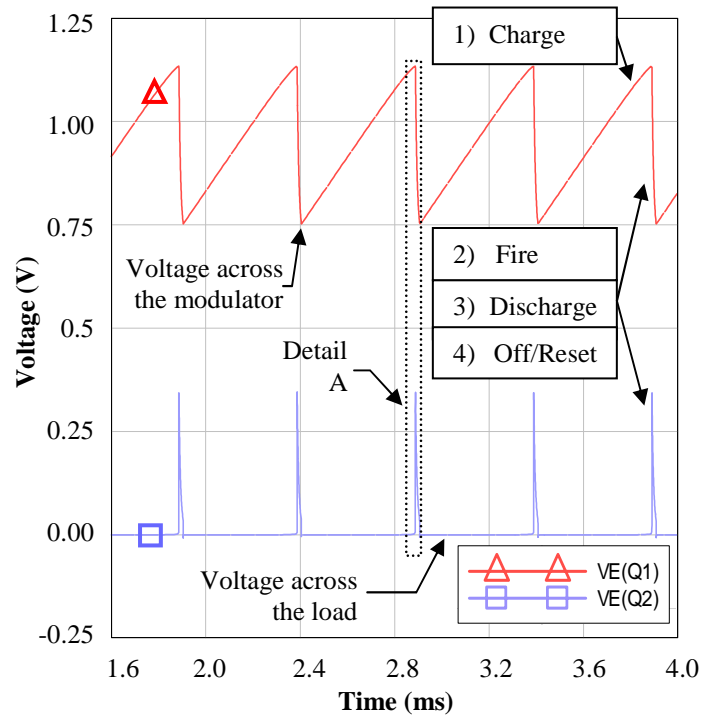


Figure 7a. Illustration of the four distinct phases of the threshold modulator cycle

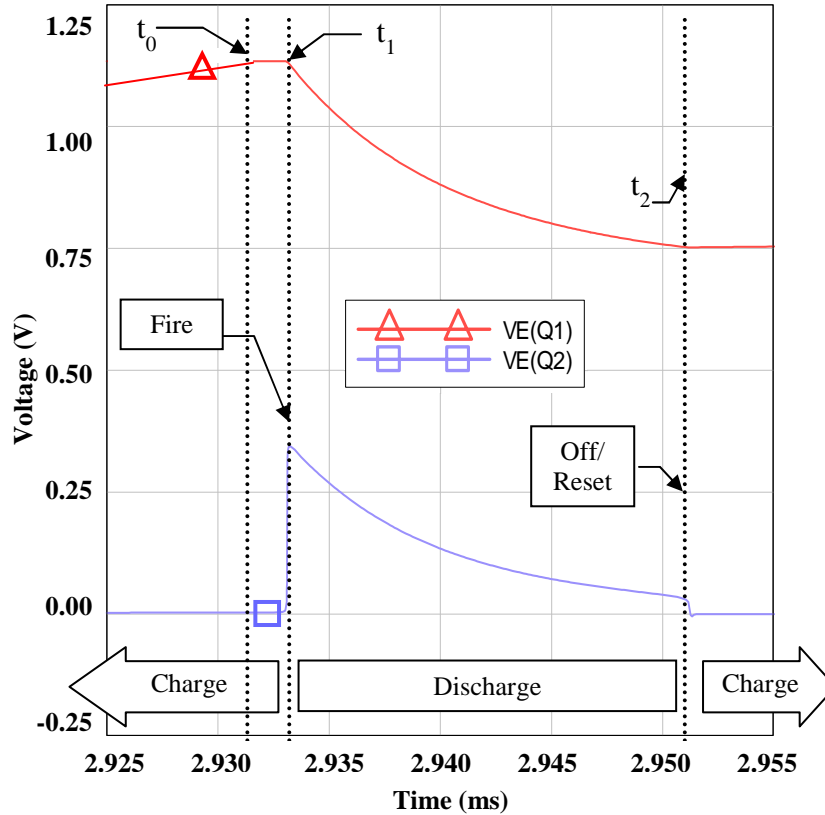


Figure 7b. Detail A: detail of the output pulse of the threshold modulator

Charging, $t < t_0$:

For each cycle; at time less than t_0 both transistors are in their relative off state and the voltage rises as a function of time. The current through the threshold modulator I_x remains relatively small so the voltage across the load resistor R_1 is negligible and the voltage potential across the capacitor, approximately equal to V_x , increases as charge is stored.

$$\frac{dV_x}{dt} = \frac{I_o}{C_e} \quad \text{Equation 2.}$$

where V_x is the voltage across the capacitors, I_o is the source current, and C_e is the combined capacitance of the stack and the modulator. During this time all the current from the piezoelectric stack enters the capacitor C_e .

Fire, $t_0 < t < t_1$

Once the voltage across the modulator reaches approximately 1.2 V, both transistors become weakly active and a small amount of current begins to flow through the modulator. When the transistors are in their active state, incremental changes in voltage and current can be modeled by the linear circuit model in Figure 8.

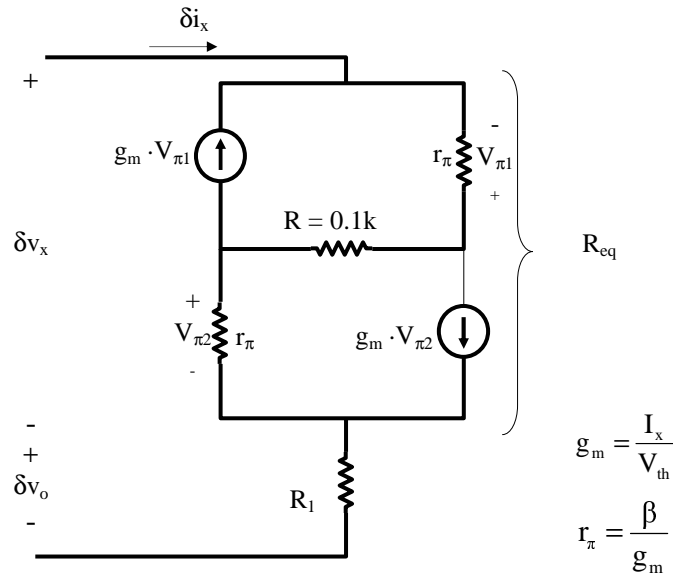


Figure 8. Incremental model of modulator for: $t_0 < t < t_1$

The constant g_m depends upon the full current I_x which is changed by increments δi_x . For sufficiently large values of I_x , R_{eq} becomes negative. This means that increasing

I_x , (positive δi_x) causes decreasing V_x (negative δv_x). If transients are short compared to the RC time constant, the voltage across the capacitor C_e does not change and decreasing V_x causes I_x to increase again. This causes V_x to collapse until it becomes small enough that Q_1 and Q_2 change from active to saturated at $t = t_1$.

This whole process starts when R_{eq} becomes negative. Analysis of the circuit in Figure 8 gives

$$R_{eq} \cong \frac{1}{g_m} \left(\frac{2}{g_m \cdot R} - 1 \right) = \frac{V_{th}}{I_x} \left(\frac{2 \cdot V_{th}}{I_x \cdot R} - 1 \right) \quad \text{Equation 3a.}$$

Thus the value of I_x that triggers the process will be

$$I_x = \frac{2 \cdot V_{th}}{R} = I_{x \min} \quad \text{Equation 3b}$$

Once I_x meets this minimum value it increases rapidly until the transistors enter saturation. The collapse of V_x occurs very rapidly, limited only by the small parasitic capacitances within the transistors. During this time the voltage across C_e remains roughly constant, and since it is constant, the capacitor is drawing relatively small current. Thus $I_o = I_x$ and the value of $I_{x \min}$ that just triggers the V_x collapse is $I_{o \min}$, which is the minimum current at which the modulator will effectively measure charge, thus putting a constraint on the minimum pressure ramp rate. In summary

$$I_{o \min} = \frac{2 \cdot V_{th}}{R} \quad \text{Equation 4.}$$

Discharge, $t_1 < t < t_2$

Once the voltage across the modulator drops to roughly 0.8 volts, both transistors are in the saturation region and the transistors can be modeled as a pair of voltage sources (Figure 9). At this time the charge stored in the capacitor and piezoelectric stack begins to flow through the modulator. During this time the base-emitter voltages of both transistors are approximately 0.7V and the collector-emitter voltages are approximately 0.1V. This model can be collapsed to a single voltage source of 0.8 V which can be defined as V_m .

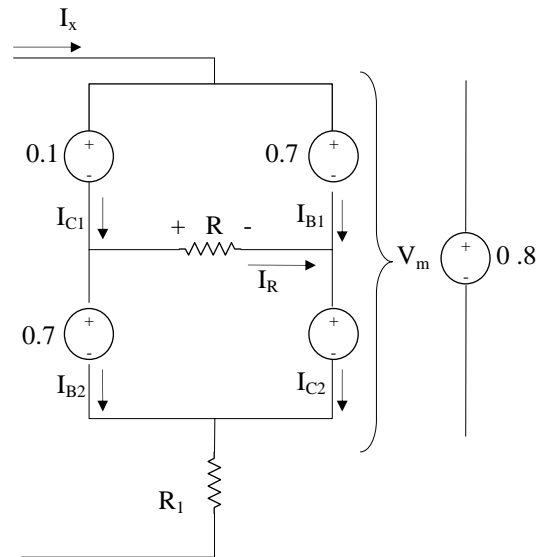


Figure 9. Circuit model of modulator when the transistors are in the saturated state: $t_1 < t < t_2$

The circuit can then be evaluated for the voltage V across the capacitor for this time period.

$$V(t) = V_m + I_o \cdot R_1 + [V(t_1) - V_m - I_o \cdot R_1] \cdot e^{-\frac{(t-t_1)}{R_1 \cdot C_e}} \quad \text{Equation 5a.}$$

$$I_x(t) = I_o + \left[\frac{V(t_1) - V_m - I_o \cdot R_1}{R_1} \right] \cdot e^{-\frac{(t-t_1)}{R_1 \cdot C_e}} \quad \text{Equation 5b.}$$

where $V(t_1)$ is the voltage across the capacitor at the start of this time period. This is roughly the same voltage as at the beginning of the V_x collapse described previously (about 1.2 volts). As the voltage across the capacitor drops the current (I_x) through the modulator also drops, which causes the transistors to move from the saturated region to the borderline between saturated and active. While saturated, $I_B \cdot \beta \geq I_c$, where β is the transistor current gain, with equality occurring at the borderline between saturation and active. Using the model in Figure 9 and setting $I_B \cdot \beta = I_c$, one can solve for $I_x = I_{x,Shutoff}$

$$I_{R,Shutoff} = I_{C1} - I_{B2} = \frac{I_x \cdot \beta}{\beta + 1} - \frac{I_x}{\beta + 1} \approx I_x \approx I_{x,Shutoff} \quad \text{Equation 6.}$$

where β is much greater than 1. By summing voltages around the loop including R in Figure 9 and using Ohm's law, $I_R = 0.6/R$

$$I_{x,Shutoff} = \frac{0.6}{R} \quad \text{Equation 7.}$$

By examining equation 5b it is clear that if the current I_o is greater than $I_{x,shutoff}$, I_x will never become small enough to shut off the modulator and the circuit will no longer measure charge. Once the current through the modulator reaches the shutoff current, the transistors go back into the active state and the reverse of what occurred between time t_0 and t_1 occurs. The equivalent resistance increases to the modulator's relative off state and the capacitive elements again begin to charge.

The above analysis explains the behavior of the modulator and also suggests the operating limits associated with stable oscillation, beyond which the modulator will not correctly measure charge.

Discussion of Performance of the Threshold Modulator

As discussed earlier, the main function of the threshold modulator is to digitize the analog pressure information that has been stored in the form of charge on the capacitive element. The digital signal consists of a train of pulses, each representing a pressure change of an amount proportional to the threshold of the modulator. There are two general categories of primary performance characteristics associated with the threshold modulator: 1) the limiting conditions under which the modulator will operate, such as temperature and current, 2) the parameters describing the shape of the output waveform used to excite the ultrasonic transmitter, such as rise time and pulse height.

Limiting Conditions

The operating temperature of the device is largely a function of package design, which is not directly within the scope of this paper; however it should be noted that temperature influences the electrical characteristics of both the piezoelectric stack and the threshold modulator. For this reason, care must be taken in the package design of this sensor to thermally decouple the sensor from the plastic melt. The temperature of the plastic typically varies as much as 240 degrees C [9, Pg. 334] while the bulk temperature of the mold is held fairly constant at temperatures ranging typically from 20 to 50 degrees C [10]. Because of the significant difference in thermal conductivity of the plastic and the mold material, usually steel or aluminum, the temperature of the interface is largely

dominated by the bulk temperature of the mold and can for most applications be maintained below 50 degrees C [11]. It has been shown by [11] that with careful package design and prudent mold cooling, the temperature will not greatly affect the performance of the piezoelectric stack or the threshold modulator.

The *operating current* (I_o) of the device can be defined by the charge per second produced by the piezoelectric stack and is directly proportional to the *pressure ramp rate* as shown by Equation 1 [5]. For the threshold modulator, there is a practical *operating current* limit under which the modulator leaks current and doesn't fire (Equation 4). This *threshold current*, represented in Figure 4 is important to the design of the threshold modulator because it reflects a *pressure ramp rate* below which a pressure change in the mold cavity will not be measured. There is also an operating current above which the threshold modulator will not fire (Equation). This *shutoff current* is important to the design of the threshold modulator because it reflects a *pressure ramp rate* above which a pressure change in the mold cavity will not be measured.

The value of the resistor R was temporarily set to $2k\Omega$ and the threshold and shutoff currents were determined from the above analysis and compared to a simulation. The analysis and simulation agree that lower current limit of the modulator with a resistance R of $2k\Omega$ and the transistors specified in Figure 5 is 0.025ma and the corresponding upper current limit is 0.30ma. Reasonable upper and lower current limits depend on the application and the requirements of the machine being controlled. However, if the *operating range* of the modulator is defined as the relative difference between the *threshold current* and the *shutoff current* it is in general better to have a

wider operating range and a smaller *threshold current*. As discussed in the above analysis these values depend on the value of the resistor R.

Output Waveform

The ultrasonic transmitter represented in Figure 5 as load R_1 and described in [12] can, for the purposes of the threshold modulator design, be thought of as a simple LRC network with a fundamental frequency between 2 MHz and 5 MHz. In the ideal case, the output pulse from the threshold modulator will excite only the fundamental frequency of the ultrasonic transmitter. The frequencies that are excited by output pulse are largely dependant on the shape of that pulse [4]. This shape, shown in Figure 7a and Figure 7b, can be described primarily by two parameters: 1) the rise time of the pulse and 2) height of the pulse. The pulse height is defined as the maximum voltage of the pulse and the rise time is defined as the time it takes the pulse to rise from 10% to 90% of the pulse height.

In order to best excite the fundamental frequency of the transmitter, the rise time should be equal to the time it takes for one quarter of the transmitter's cycle [13]. For a 5MHz transmitter, this corresponds to a rise time of 50ns. It is possible to lengthen the rise time of the output waveform using a passive filter such as an inductor but it is not possible to shorten it using such a passive filter (which is a requirement of an un-powered sensor). It is therefore a requirement for the output pulse to have a rise time of no more than 50ns to excite an ultrasonic transmitter at 5MHz. Comparatively, the rise time of the above simulation is approximately 36ns, adequate for the required excitation.

Bench Top Device and Comparison to Simulation

A prototype of the above circuit was built using a Keithley 2400 source meter in place of the ideal current source with a current of 0.30 mA corresponding to a 100 MPa/s ramp rate on a 10 disk stack. The voltages in the circuit were measured using a Tektronix 3012 100 M Ω digital oscilloscope. The input and output voltages were measured between the emitter of Q1 to ground and the emitter of Q2 to ground respectively. The experimental and simulation results of a transient analysis of the specific model given in Figure 5 are presented in Figure 10 and Figure 11.

Figure 10 shows the voltage output for the simulation and the experimental results. Each pulse represents a pressure change of 43.8 kPa, corresponding to 0.044% of a possible 100 MPa pressure range (approximately 11 bit accuracy). The current source was switched on at time $t = 0$ and the circuit began stable oscillation at approximately 0.225 ms; after reaching the threshold voltage.

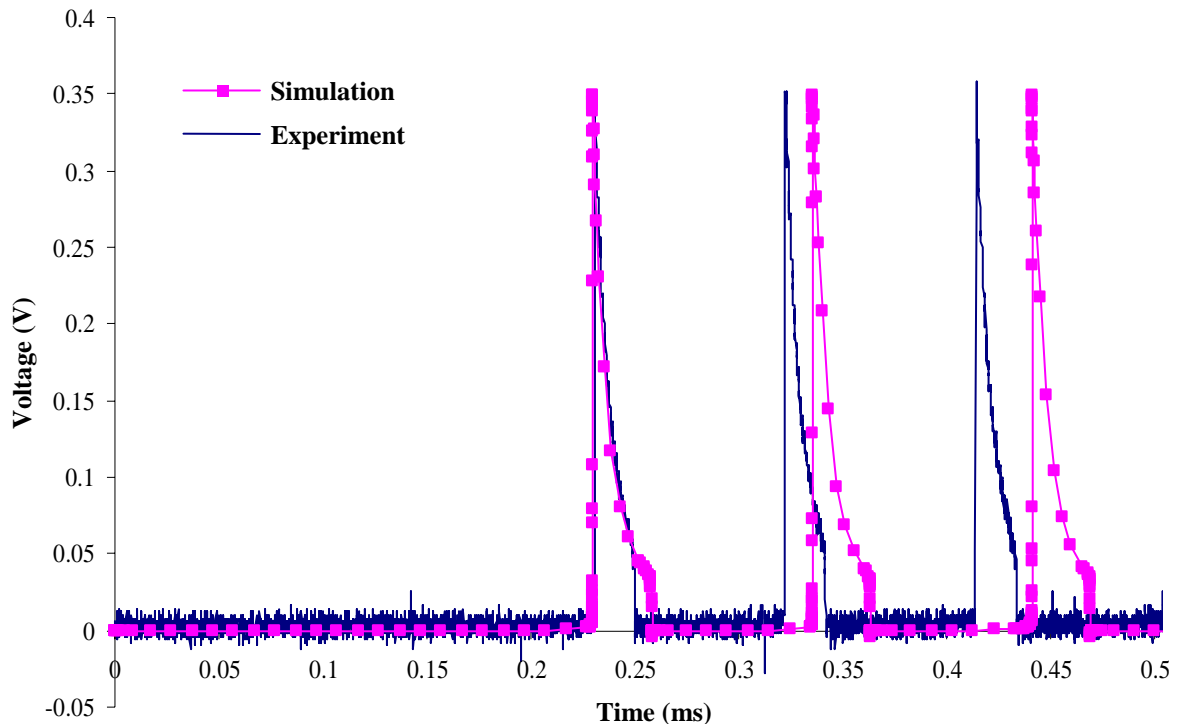


Figure 10. Transient experimental and simulation results for the threshold modulator

The experimental results matched very closely that of the simulation. The observed pulse height agrees within about 3% of the prediction, while the total pulse width varies by about 25% (Figure 11). This discrepancy is from a difference in the *lower threshold voltages* of the transistors used in the simulation and those used in the experiment. While this difference changes the timing of the circuit, it has a negligible effect on the performance parameters. The corresponding rise time is approximately 40 ns, which implies that the output pulse if directly connected to an acoustic transmitter would be able to effectively excite a 6.25 MHz mode of vibration. This performance is above the proposed operating frequency (5MHz) of an acoustic transmitter designed for acoustic telemetry in injection molding [14].

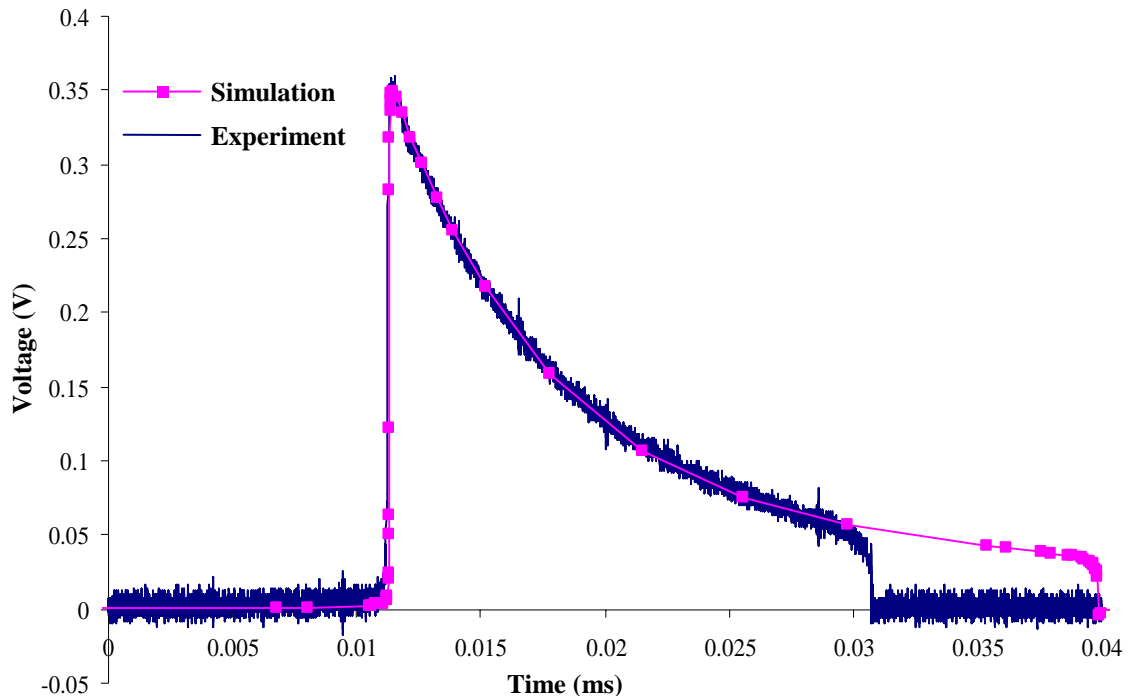


Figure 11. Comparison of the experimentally measured and simulated output pulses

Optimization of threshold modulator bench top device

An optimization of the bench top prototype circuit was carried out in order to improve the performance parameters of the modulator. Seven off-the-shelf PNP and five off-the-shelf NPN switching transistors (Table 1) were evaluated in a full factorial design of experiments (DOE). At each experiment in the 36 run DOE the clamp resistor (R) was adjusted to set the threshold pressure ramp rate at approximately 0.3mA. For this configuration the highest shutoff ramp rate represents the largest the operating range.

Throughout the experiment the upper cutoff limit varied from 1.2 mA to 2.6 mA, effectively increasing the ability to measure charge 2.5 times.

Table 1. The design variables for an optimization comparing the performance of seven PNP and five NPN off-the-shelf transistors.

Optimized design variables for full factorial DOE	
PNP Transistor	NPN Transistor
pn3638	2n4401
2n4403	pn4275
bc327	bc549
bc559	2n3904
2n4125	bc547
bc212	
2n3906	

The Fairchild PNP BC212 transistor coupled with the National Semiconductor NPN PN4275 resulted in the largest operating range modulator 0.3mA to 2.6mA. This modulator will effectively measure pressure changes ranging from about 1MPa/s to 8.3MPa/s when used with the 10 disk stack previously discussed. This circuit should be the starting point for an optimization involving the energy extraction device, threshold modulator, ultrasonic transmitter, and ultrasonic receiver.

Conclusions and Future Work

An un-powered device consisting of a pair of bipolar junction transistors designed to control the flow of charge between an energy extraction device and an ultrasonic transmitter has been discussed, modeled, simulated, constructed, and optimized. The discussion and evaluation of the threshold modulator with respect to the predicted limits

under which the device will operate. Results from simulation and bench top experiments agree; the Threshold current (lower limit) and shutoff current (upper limit) described in equations 4 and 7 respectively can be controlled by varying the value of the resistor R. An optimization of the bench top device was performed in order to determine the combination of readily available switching transistors that produced the best upper and lower current limits.

The output waveform produced by the threshold modulator was also discussed with respect to predictions from the simulation and the bench top experiments. The rise time and the height of the output pulse is consistent across the simulation and experiment and will be sufficient to excite an ultrasonic transmitter at frequencies exceeding 5MHz which can drive the proposed transmission frequencies of between 2MHz and 4MHz.

In the future it will be necessary to evaluate methods of increasing the operating range of the modulator such as a non-linear resistor in place of R. A resistance element with an increased resistance at lower currents, in order to reduce the lower current limit, and a decreased resistance at higher currents, in order to increase the upper current limit, should be evaluated. In addition to a wider operating range, an investigation of how to increase the output pulse amplitude will be undertaken in order to have better controllability of the ultrasonic transmission process. Finally, an integration of each of the sensor subsystems will be made.

Acknowledgement

The authors gratefully acknowledge funding provided to this research by the National Science Foundation under DMI-9988757.

Bibliography

- [1] National Research Council (U.S.). Unit Manufacturing Process Research Committee., *Unit manufacturing processes : issues and opportunities in research*. Washington, D.C.: National Academy Press, 1995.
- [2] I. A. Rawabdeh and P. F. Petersen, "In-Line Monitoring of Injection Molding Operations: A Literature Review," *Injection Molding Technology*, vol. 3, pp. 47-53, 1999.
- [3] B. Watkins, "Five Myths about Sensing Mold Pressure," in *Sensors Magazine*, vol. 14, 1997, pp. 73-78.
- [4] L. E. Kinsler, *Fundamentals of acoustics*, 3rd ed. New York: Wiley, 1982.
- [5] C. Theurer, L. Zhang, D. Kazmer, and R. Gao, "Self-Energized Wireless Pressure Sensor Using Energy Extraction from Injection Mold Pressure Differential," presented at Proceedings of IEEE Sensors, Orlando, FL, 2002.
- [6] N. Chubachi and H. Kamata, "Various equivalent circuits for thickness mode piezoelectric transducers," *Electronics & Communications in Japan, Part II: Electronics (English translation of Denshi Tsushin Gakkai Ronbunshi)*, pp. 50-59, 1996.
- [7] J. Van Randerlaat and R. E. Settingington, *Piezoelectric ceramics*, 2d ed. London: Mullard, 1974.
- [8] C. Theurer, "Energy Extraction for a Self-Energized Pressure Sensor," To Appear *IEEE Sensors*, December 2003.
- [9] N. G. McCrum, C. P. Buckley, and C. B. Bucknall, *Principles of polymer engineering*, 2nd ed. Oxford ; New York: Oxford University Press, 1997.
- [10] C. Theurer, L. Zhang, D. Kazmer, and R. Gao, "Threshold Energy Switching and its Application to Wireless Sensing in High Energy Manufacturing Processes," presented at ASME International Mechanical Engineering Congress and Exhibition (IMECE), Symposium on Intelligent Sensors, New Orleans, LA, 2002.
- [11] C. Theurer, L. Zhang, D. Kazmer, and R. Gao, "Evaluation of a piezoelectric energy extraction device for cavity pressure sensing in injection molding," presented at ASME International Mechanical Engineering Congress and Exhibition, Washington, D.C, 2003.
- [12] L. Zhang, C. Theurer, R. Gao, and D. Kazmer, "Design of a wireless sensor for injection molding cavity pressure measurement," presented at ASME International Mechanical Engineering Congress and Exhibition, New York, NY, 2001.

- [13] C. S. Desilets, J. D. Fraser, and G. S. Kino, "Design of Efficient Broad-Band Piezoelectric Transducers," *IEEE Transactions on Sonics and Ultrasonics*, vol. SU-25, pp. 115-125, 1978.
- [14] L. Zhang, C. Theurer, R. Gao, and D. Kazmer, "Frequency Design of an Ultrasonic Transmitter for Injection Molding Pressure Measurement," *NAMRI*, vol. 31, 2003.